# Chapter 1

# Shell Model: Woods–Saxon Potential and Ground-State $J^\pi$

*"For realistic calculations, more accurate potentials are preferred... Among the various models, the Woods–Saxon potential is particularly effective."*
lecture notes, PH5001

Lecture 12 showed that magic numbers beyond 20 require spin–orbit coupling, and that the choice of infinite well versus harmonic oscillator does not change those magic numbers once $\boldsymbol{\ell} \cdot \boldsymbol{s}$ is strong enough. Realistic calculations still need a finite, diffuse mean field: the **Woods–Saxon** potential. With that spectrum one reads ground-state spin and parity from the extreme single-particle filling rules [6, 1, 10].

## 1.1 Why infinite potentials fail as absolute models

An infinite wall forbids nucleon removal: separation energies would be infinite. Real nuclei have finite $S_n$ and $S_p$. A finite square well allows separation but retains a discontinuous edge. Nuclear density and the mean field fall smoothly over a surface thickness of order 2–3 fm (Lecture 2). The potential should follow that density.

## 1.2 Woods–Saxon single-particle potential

Woods and Saxon introduced this radial shape as the real part of a diffuse *optical-model* potential for nucleon–nucleus scattering [10]. Its finite depth and smooth surface also make it a useful phenomenological bound-state mean field; that later use is not a first-principles derivation. The standard central form is

$$V_{\mathrm{WS}}(r) = -\frac{V_0}{1 + \exp\big[(r-R)/a\big]}, \tag{1.1}$$

with $R = r_0 A^{1/3}$, $r_0 \approx 1.25\,\mathrm{fm}$, diffuseness $a \approx 0.5$–$0.7\,\mathrm{fm}$, and depth $V_0 \sim 50\,\mathrm{MeV}$ chosen to match separation energies [10, 6, 1]. The potential is nearly flat and attractive in the nuclear interior, then rises smoothly through the surface to zero outside. At $r = R$ one has $V = -V_0/2$.

The 10%–90% surface thickness follows directly from the Woods–Saxon shape. Define

$$f(r) = \frac{-V_{\mathrm{WS}}(r)}{V_0} = \frac{1}{1+\exp[(r-R)/a]}.$$

Solving $f(r) = p$ gives

$$\frac{1}{p} - 1 = e^{(r-R)/a}, \qquad r(p) = R + a\ln\left(\frac{1-p}{p}\right). \tag{1.2}$$

Thus the inner 90% point and outer 10% point are

$$r(0.9) = R - a\ln 9, \qquad r(0.1) = R + a\ln 9. \tag{1.3}$$

Their radial separation is

$$t = r(0.1) - r(0.9) = 2a\ln 9 = 4a\ln 3 \approx 4.4\,a, \tag{1.4}$$

of order 2–3 fm for realistic $a$.

The radial Schrödinger equation for the reduced wave function $u(r)$ is

$$-\frac{\hbar^2}{2m}\frac{\mathrm{d}^2u}{\mathrm{d}r^2} + \left[V_{\mathrm{WS}}(r) + \frac{\ell(\ell+1)\hbar^2}{2mr^2}\right]u = E\,u, \tag{1.5}$$

with $u(0) = 0$. Outside the nucleus, $V \to 0$ for a neutron. It is useful to combine the potential and centrifugal terms into

$$V_{\mathrm{eff}}(r) = V_{\mathrm{WS}}(r) + \frac{\ell(\ell+1)\hbar^2}{2mr^2}. \tag{1.6}$$

For $\ell > 0$, the positive centrifugal barrier suppresses the wave function near the origin and shifts probability toward the nuclear surface. Far outside, both terms approach zero. The radial equation then reduces to

$$\frac{\mathrm{d}^2u}{\mathrm{d}r^2} = \frac{2m|E|}{\hbar^2}u = \kappa^2 u \qquad (E < 0), \tag{1.7}$$

whose two solutions are $e^{+\kappa r}$ and $e^{-\kappa r}$. Normalisability eliminates the growing solution, leaving

$$u(r) \underset{r\to\infty}{\longrightarrow} C\,e^{-\kappa r}, \qquad \kappa = \sqrt{\frac{2m|E|}{\hbar^2}}. \tag{1.8}$$

Matching the interior numerical solution to this exterior exponential quantises the allowed energies. There is therefore a finite number of bound orbits, and the least-bound nucleon has a realistic separation energy of a few to tens of MeV.

The decay length $1/\kappa \propto 1/\sqrt{|E|}$ is important physics: a weakly bound neutron has a long exterior tail. Near the neutron drip line this produces diffuse skins and, for low $\ell$ where the centrifugal barrier is small, halo structure. A bound proton also decays, but its asymptotic tail is modified by the repulsive Coulomb potential rather than being a pure exponential at finite radius.

For protons one must add the Coulomb potential of the remaining charge distribution. A simple estimate for a uniformly charged sphere of radius $R$ is

$$V_{\mathrm{C}}(r) = \begin{cases} \dfrac{(Z-1)e^2}{8\pi\epsilon_0 R}(3 - r^2/R^2), & r \le R, \\ \dfrac{(Z-1)e^2}{4\pi\epsilon_0 r}, & r > R. \end{cases} \tag{1.9}$$

Consequently the effective proton potential is raised and is less binding than the neutron potential at the same $A$. It is misleading to call the Woods–Saxon geometry itself "wider": the Coulomb tail is long-ranged, while the spatial extent of an orbital depends on its binding and angular momentum. Coulomb repulsion is one reason heavy stable nuclei require $N > Z$ [6, 1].

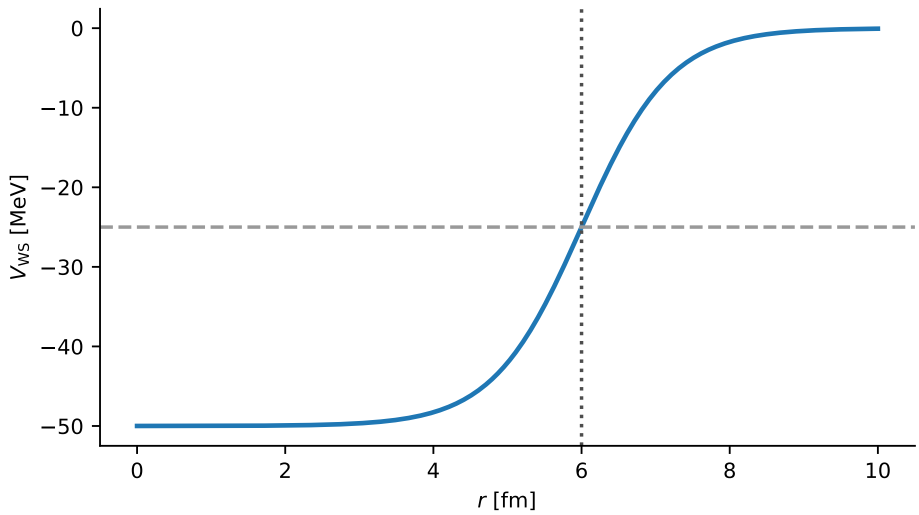


**Figure 1.1:** Woods–Saxon potential $V(r)$ used as the basic single-particle nuclear mean field. The red marker indicates the half-depth radius $R$ (original vector evaluation of the analytic form; Woods and Saxon [10]).

## 1.3 From oscillator to Woods–Saxon to spin–orbit

Compared with the oscillator, a finite diffuse well lowers high-$\ell$ orbitals preferentially (they live nearer the surface) and lifts accidental degeneracies such as $1d$–$2s$ and $1f$–$2p$. Typical trends when passing from oscillator (HO) to Woods–Saxon (WS) before spin–orbit:

- $1f$ drops more than $2p$;
- $1g$ drops strongly, approaching the $1f, 2p$ region;
- $1d$ and $2s$ split, with $1d$ usually lower;
- $2d$ and $3s$ descend; the uppermost level becomes $1h$.

Adding $\boldsymbol{\ell} \cdot \boldsymbol{s}$ then splits each $\ell > 0$ level: $1p \to p_{3/2}, p_{1/2}$; $1d \to d_{5/2}, d_{3/2}$; $1f \to f_{7/2}, f_{5/2}$; $1g \to g_{9/2}, g_{7/2}$; $1h \to h_{11/2}, h_{9/2}$. The magic numbers remain $2, 8, 20, 28, 50, 82, 126$, but the detailed spacings become realistic (Fig. 1.2).

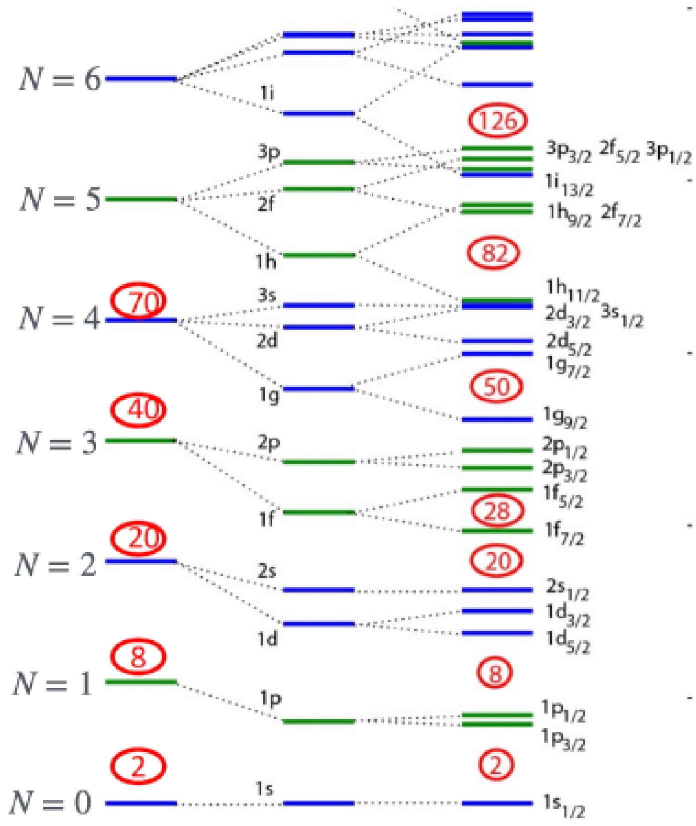


**Figure 1.2:** Single-particle spectrum: harmonic oscillator (HO), Woods–Saxon (WS), and Woods–Saxon plus spin–orbit (WS+LS). Red circles mark shell closures (adapted from the original PH5001 lecture figure; cf. Dunlap [1] and Krane [6]).

**Key idea**

Magic numbers are robust once spin–orbit is present. Energy values and intra-shell ordering depend on the central potential; Woods–Saxon is the standard realistic choice. The finite depth controls separation energies, the diffuseness controls surface physics, the centrifugal term separates different $\ell$, and spin–orbit coupling separates $j = \ell \pm \frac{1}{2}$.

## 1.4 Extreme single-particle model

In the **extreme single-particle** (or independent-particle) limit one assumes:

1. nucleons fill the lowest available single-particle orbits;
2. residual interactions are dominated by pairing of like nucleons into $J = 0$ pairs;
3. ground-state properties of odd-$A$ nuclei (spin, parity, magnetic moment) are carried by the last unpaired nucleon.

Even–even nuclei then have all nucleons paired. The model is most reliable near closed shells; mid-shell, configuration mixing and collective motion become essential (Lecture 15).

## 1.5 Spin and parity: notation

Nuclear "spin" means total angular momentum $\boldsymbol{I}$ (often written $J$). For a single nucleon,

$$\boldsymbol{j} = \boldsymbol{\ell} + \boldsymbol{s}, \qquad |j| = \sqrt{j(j+1)}\,\hbar, \qquad \pi = (-1)^\ell. \tag{1.10}$$

The spectroscopic label is $I^\pi$ (or $J^\pi$). Example: a nucleon in $d_{5/2}$ ($\ell = 2$, $j = \frac{5}{2}$) has $I^\pi = \frac{5}{2}^+$.

## 1.6 Even–even ground states and paired $0^+$ structure

In the paired mean-field limit, like nucleons occupy time-reversed states and couple predominantly to total angular momentum zero. Consider two identical nucleons in the same $n\ell_j$ orbit. The Pauli principle restricts the allowed total angular momenta of the pair to the even values

$$I = 0, 2, \ldots, 2j - 1 \tag{1.11}$$

(odd multipoles are excluded for two identical fermions in one $j$ shell). Among these, the residual short-range attraction favours the maximum spatial overlap, which occurs for the $I = 0$ pair. That pair has positive parity regardless of whether $\ell$ is even or odd, because

$$\pi_{\text{pair}} = (-1)^\ell (-1)^\ell = +1. \tag{1.12}$$

If the even–even ground state is dominated by this paired structure,

$$I^\pi = 0^+, \tag{1.13}$$

independent of which orbits are filled. Observed even–even nuclear ground states are $0^+$, but that empirical rule is not proved merely by particle counting: deformation and configuration mixing can make the wave function highly correlated while preserving $0^+$ [6, 1, 20]. The magnetic moment vanishes as well (Lecture 14).

## 1.7 Odd-$A$ nuclei: last nucleon rules

Either $Z$ or $N$ is odd. All but one nucleon form $J = 0$ pairs; the unpaired nucleon occupies the last partially filled orbit $n\ell_j$ and determines

$$I = j, \qquad \pi = (-1)^\ell. \tag{1.14}$$

### 1.7.1 Example: $^{15}$N

Nitrogen-15 has $Z = 7$, $N = 8$. Neutrons fill a closed shell through $1p_{1/2}$. The proton occupation is

$$(1s_{1/2})^2(1p_{3/2})^4(1p_{1/2})^1. \tag{1.15}$$

The unpaired proton is in $1p_{1/2}$ ($\ell = 1$, $j = \frac{1}{2}$), so

$$I^\pi = \tfrac{1}{2}^-, \tag{1.16}$$

in agreement with experiment.

### 1.7.2 Nearby configurations and mixing: $^{61}$Ni

Nickel-61 has $Z = 28$, $N = 33$. The protons fill the closed $Z = 28$ shell. Above the $N = 28$ neutron core one must place five valence neutrons in the $2p_{3/2}$, $1f_{5/2}$ and $2p_{1/2}$ sequence. Two limiting basis configurations illustrate the role of residual interactions:

$$(2p_{3/2})^4(1f_{5/2})^1 \quad \Rightarrow \quad I^\pi = \tfrac{5}{2}^-, \tag{1.17}$$
$$(2p_{3/2})^3(1f_{5/2})^2 \quad \Rightarrow \quad I^\pi = \tfrac{3}{2}^-. \tag{1.18}$$

In the second basis configuration the two $1f_{5/2}$ neutrons can form a $J = 0$ pair, leaving the odd neutron in $2p_{3/2}$. Experiment finds $I^\pi = \frac{3}{2}^-$ for the ground state of $^{61}$Ni [20, 21, 6]. This fixes the total quantum numbers, not a unique occupation: the physical state is a shell-model superposition of nearby configurations with $I^\pi = 3/2^-$, including core-coupled pieces.

The lesson is not a universal rule that "pairing is always stronger in high-$\ell$ orbits", but rather that residual pairing and configuration mixing can reorganise nearby basis states when single-particle spacings are small. The extreme model supplies useful labels, while spectroscopic factors and a full diagonalisation test their purity [6, 1].

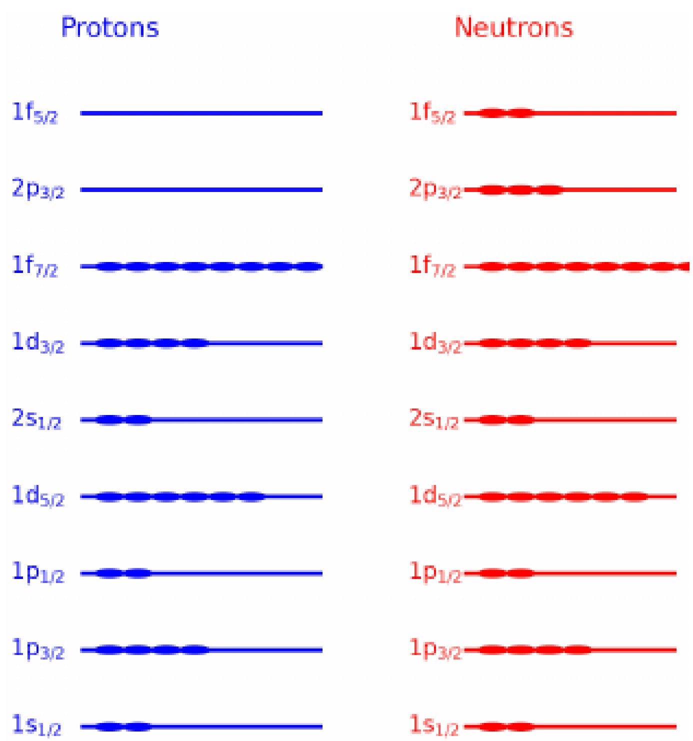


**Figure 1.3:** One limiting $^{61}$Ni valence configuration, $(2p_{3/2})^3(1f_{5/2})^2$, compatible with a $3/2^-$ odd neutron. The evaluated ground-state spin is $3/2^-$, but the physical wave function mixes this and other $3/2^-$ configurations [20, 21].

### 1.7.3 Example: $^{17}$O

Oxygen-17 ($Z = 8$, $N = 9$) has closed proton shells and neutrons $(1s_{1/2})^2(1p_{3/2})^4(1p_{1/2})^2(1d_{5/2})^1$ (Fig. 1.4). The valence neutron is $1d_{5/2}$, so

$$I^\pi = \tfrac{5}{2}^+. \tag{1.19}$$

Evaluated data confirm the ground state $5/2^+$ and a first excited $1/2^+$ state at 871 keV, corresponding to promotion of the valence neutron to $2s_{1/2}$ [20, 21]. Negative-parity states involve $p$-shell holes. Excited states of $^{17}$O are treated systematically in Lecture 15.

## 1.8 Odd–odd nuclei

Both an unpaired proton and an unpaired neutron contribute. Their angular momenta $\boldsymbol{j}_p$ and $\boldsymbol{j}_n$ couple to a multiplet of total angular momentum

$$|j_p - j_n| \le I \le j_p + j_n, \tag{1.20}$$

in integer steps, with parity

$$\pi = (-1)^{\ell_p + \ell_n}. \tag{1.21}$$

The triangle rule alone does *not* select the ground-state member of the multiplet: residual proton–neutron interactions decide the ordering. Nordheim's empirical rules provide a first guide

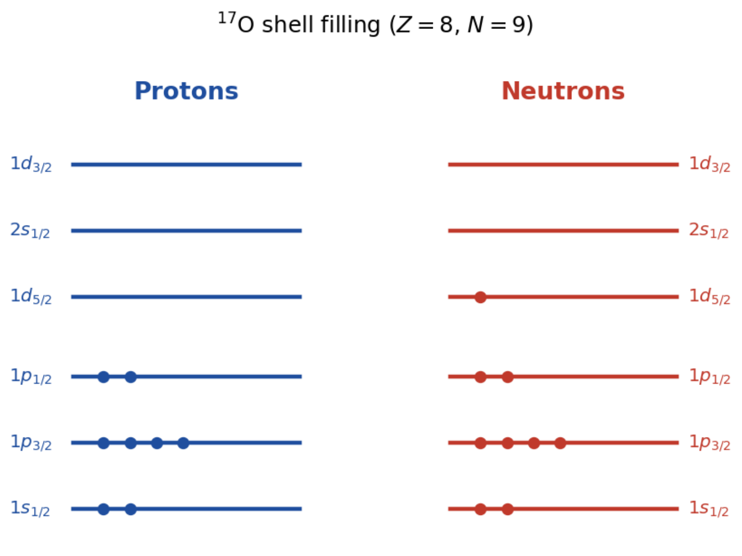


**Figure 1.4:** Shell-model level occupation for $^{17}$O: closed proton shell and unpaired $1d_{5/2}$ neutron (original lecture figure).

[19, 6], but they are not rigorous theorems. Few odd–odd nuclei are stable (Lecture 5); $^{14}$N ($I^\pi = 1^+$) is a classic light example [20].

**Key idea**

Even–even: $0^+$. Odd $A$: $I^\pi$ of the last unpaired nucleon (subject to pairing reordering near closely spaced levels). Odd–odd: an allowed multiplet $|j_p - j_n| \le I \le j_p + j_n$, with the ground member fixed by residual $pn$ interactions.

## 1.9 Pairing and the SEMF

Two nucleons in the same $j$ orbit prefer $I_{\text{pair}} = 0$. That pairing energy is the microscopic origin of the SEMF pairing term $\delta$ (Lecture 4) and of the even–even preference for stability. Breaking a pair costs $\sim$ 1–2 MeV and is the first step toward many low-lying even–even excitations (two-quasiparticle states), while odd-$A$ spectra often show the pure single-particle sequence until core excitations set in [6].

## 1.10 Deeper physics: Woods–Saxon orbits and $I^\pi$ assignments

### 1.10.1 Woods–Saxon parameters and level ordering

The Woods–Saxon well (Equation (1.1))

$$V(r) = -\frac{V_0}{1 + \exp[(r - R)/a]} \tag{1.22}$$

interpolates between $-V_0$ in the interior and zero outside, with surface diffuseness $a \approx 0.65$ fm. Solving the radial Schrödinger equation (Equation (1.5)) with a spin–orbit term yields the single-particle spectrum of Figure 1.2. The centrifugal barrier $\ell(\ell+1)\hbar^2/(2mr^2)$ raises $p$ waves relative to $s$ waves; spin–orbit further splits each $\ell$ into $j = \ell \pm \frac{1}{2}$. Near closed shells the extreme model (Lecture 13) assigns ground-state $I^\pi$ from the last unpaired nucleon.

### 1.10.2 Worked $I^\pi$ assignments

Consider $^{17}$O ($N = 9$, $Z = 8$). The closed $^{16}$O core ($N = 8$ magic) leaves one neutron outside. Filling the levels in Figure 1.2 places the valence neutron in the $1d_{5/2}$ orbit ($\ell = 2$, $j = \frac{5}{2}$). Parity is $(-1)^\ell = +$, so

$$I^\pi(^{17}\mathrm{O}) = \tfrac{5}{2}^+, \tag{1.23}$$

matching ENSDF [20, 6]. For $^{15}$N ($N = 7$, one proton hole on $^{16}$O), the last unpaired proton occupies $1p_{1/2}$ ($\ell = 1$, $j = \frac{1}{2}$), giving $I^\pi = \frac{1}{2}^-$.

**Key idea**

**Assignment checklist.**

1. Identify the closed core (magic $N$ or $Z$).
2. Locate the last partially filled orbit in the WS diagram.
3. Read $I = j$ and $\pi = (-1)^\ell$ for a single unpaired nucleon.
4. Flag mid-shell nuclei ($^{61}$Ni, etc.) where configuration mixing invalidates step 3.

**Remark**

**Protons vs neutrons.** Coulomb repulsion raises proton levels relative to neutron levels at the same $A$, so mirror nuclei are similar but not identical. Transfer reactions measure proton and neutron spectroscopic factors separately (Lecture 15 further material). Woods–Saxon is a starting map, not the final word for drip-line nuclei where the continuum must be included.

### 1.10.3 Centrifugal barrier and orbit ordering

The radial equation (Equation (1.5)) includes $\ell(\ell+1)\hbar^2/(2mr^2)$, which raises $p$-wave orbits above $s$-waves and $d$-waves above $p$-waves at the same $n$. Combined with spin–orbit splitting, this produces the familiar ordering $1s_{1/2}, 1p_{3/2}, 1p_{1/2}, 1d_{5/2}, \ldots$ of Figure 1.2. Assigning $I^\pi$ is then a bookkeeping exercise *provided* the last nucleon sits in a orbit separated from neighbours by more than the residual interaction scale ($\sim$ 1–3 MeV near closed shells, larger mid-shell) [6, 20].

### 1.10.4 From orbits to transfer-reaction quantum numbers

One-nucleon transfer reactions (Lecture 15) populate the same orbits with angular-momentum transfer $\Delta L = \ell$ fixed by the reaction mechanism. If $^{17}$O is truly $1d_{5/2}$, a $(d, p)$ cross section on $^{16}$O should peak at the angular momentum matched to $\ell = 2$. Mismatch between angular distributions and the WS assignment signals configuration mixing ($^{61}$Ni is the standard cautionary example) [1, 6].

### 1.10.5 Parity and allowed $I^\pi$ combinations

For a single nucleon, $\pi = (-1)^\ell$. Even–even ground states are $0^+$ (Section 1.6). Odd–odd nuclei require coupling of two unpaired nucleons and can have $I^\pi$ values not accessible to a single orbit (for example $0^-$ from $p_{1/2} \otimes p_{1/2}$). The extreme model's last-nucleon rule applies only to odd-$A$ nuclei; attempting to assign odd–odd ground states from one orbit alone is a common student error [6, 20].

**Surface thickness**

For diffuseness $a \simeq 0.6\,\mathrm{fm}$, the 10%–90% skin thickness is $t = 4a \ln 3 \simeq 2.6\,\mathrm{fm}$, matching Lecture 1's empirical surface. Changing $a$ at fixed central depth moves single-particle orbitals differently for low-$\ell$ and high-$\ell$ states because of their radial weighting at the surface.

Configuration mixing in mid-shell nuclei fragments the single-particle strength: the spectroscopic factor to a given final state can be $\ll 1$ even when a naive filling diagram suggests a pure orbital. Always treat lecture $I^\pi$ rules as the first guess, then look for nearby levels of the same parity that signal mixing.

### Depth-extra reinforcement for continuum orbitals

A positive-energy "bound-state" root in a truncated basis is not a resonance. Record energy and width from a continuum calculation before comparing with knockout data. This remark protects Lecture 13 assignments near drip lines from a common misreading of numerical output.

### Physics-depth close

The Woods–Saxon model is the usable mean field for $I^\pi$ assignments. Its parameters encode saturation scales from Lecture 2 and its failures encode correlation physics from Lectures 14–15. Treat every assigned $I^\pi$ as a hypothesis to check against ENSDF, not as a theorem.

### Parameter correlations and drip-line caution

Depth, radius, and diffuseness of the Woods–Saxon well are correlated when only one eigenvalue is constrained. Fitting several isotopic chains and both neutron and proton orbitals reduces that ambiguity. Spin–orbit depths are further constrained by magic-number splittings from Lecture 12. Near drip lines, a 5% depth change can unbind a weakly held orbital, so continuum methods replace naive bound-state roots. Mid-shell nuclei fragment single-particle strength: spectroscopic factors from transfer (Lecture 21) then replace the extreme last-nucleon rule. Keep a short checklist: closed core? last orbit? $I = j$ and $\pi = (-1)^\ell$? nearby same-parity levels signalling mixing? That checklist is Lecture 13's practical payload.

**Surface weighting**

High-$\ell$ orbitals weight the surface more than low-$\ell$ orbitals. Changing diffuseness at fixed central density therefore reorders levels even when the rms radius from Lecture 1 is held fixed. Surface physics and shell ordering are inseparable.

## 1.11 Further physics: proton versus neutron potentials

Because protons feel Coulomb repulsion in addition to the nuclear mean field, the proton single-particle spectrum is not identical to the neutron spectrum at the same $A$. Relative to neutrons, proton orbits are pushed upward, and the least-bound proton typically has a smaller separation energy near the proton drip line than the analogous neutron near the neutron drip line [6, 1].

In transfer and knockout reactions one therefore maps proton and neutron spectroscopic factors separately. Near closed shells the extreme single-particle assignments for $I^\pi$ remain robust; far from stability the same residual interactions that reorder $^{61}$Ni can rearrange whole sequences of levels and even dissolve traditional magic numbers. Modern shell-model and density-functional calculations keep the Woods–Saxon (or Hartree–Fock) mean field as the starting point and diagonalise a residual interaction in a truncated valence space.

### 1.11.1 Surface thickness of a Woods–Saxon potential

For $V(r) = -V_0/[1 + \exp((r - R)/a)]$, the density falls from 90% to 10% of its central value over a distance

$$t \approx 4a \ln 3 \approx 4.4a. \tag{1.24}$$

With $a = 0.65\,\mathrm{fm}$, $t \approx 2.9\,\mathrm{fm}$, comparable to the nuclear skin thickness inferred from electron scattering (Lecture 1). The radius $R \approx 1.25\,A^{1/3}\,\mathrm{fm}$ sets the bulk size; $a$ sets the diffuseness. Deeply bound orbits ($1s$, $1p$) probe the interior; weakly bound valence orbits ($1g$, $1h$) probe the surface region where $f(r)$ in the spin–orbit term peaks [6, 10].

### 1.11.2 Configuration mixing beyond the extreme model

$^{61}$Ni ($N = 33$, one neutron outside $^{60}$Ni) is often quoted as $I^\pi = \frac{3}{2}^-$ from the $1f_{5/2}$ orbit, but the full spectrum shows multiple low-lying states within hundreds of keV. Residual interactions mix $1f_{5/2}$, $2p_{3/2}$, and $2p_{1/2}$ configurations, so the last-nucleon picture is a zeroth-order guide only. The extreme model is reliable when the shell gap exceeds the residual interaction ($\Delta\varepsilon \gg V_{\mathrm{res}}$); it fails in mid-shell where $E(2^+)$ drops to tens of keV (Lecture 15) [6, 1, 20].

**Mirror pair $^{17}$O / $^{17}$F**

Both have one nucleon outside $^{16}$O. Coulomb shifts the proton levels upward, so $^{17}$F ($I = \frac{5}{2}^+$, $1d_{5/2}$ proton) mirrors $^{17}$O ($I = \frac{5}{2}^+$, $1d_{5/2}$ neutron) in $I^\pi$ but with different separation energies. The magnetic moments differ because the valence nucleon charge differs (Lecture 14): Schmidt lines apply separately to protons and neutrons [6, 20].

### 1.11.3 Bridge to Lectures 14–15

$I^\pi$ from the last nucleon (Section 1.7) is tested by magnetic moments (Lecture 14) and by transfer reactions that measure spectroscopic factors (Lecture 15). A large spectroscopic factor confirms a pure single-particle assignment; fragmentation of strength signals mixing. Near closed shells both tests usually pass; mid-shell they fail together, signalling the onset of collectivity [1].

### 1.11.4 Woods–Saxon parameters in numbers

Typical values for medium-mass nuclei are $V_0 \approx 50\,\mathrm{MeV}$, $R \approx 1.25\,A^{1/3}\,\mathrm{fm}$, $a \approx 0.65\,\mathrm{fm}$, and a spin–orbit strength that splits $1f_{7/2}$ and $1f_{5/2}$ by several MeV. For $^{208}$Pb, $R \approx 6.5\,\mathrm{fm}$ and the least-bound valence neutrons ($1i_{13/2}$, $2g_{9/2}$) sit only $\sim 5\,\mathrm{MeV}$ below continuum threshold, foreshadowing the drip-line physics discussed in the research frontier below [6, 10, 20].

## 1.12 Deeper reading: $I^\pi$, spectroscopic factors, and the continuum

The extreme single-particle picture assigns $I^\pi$ from the last odd nucleon's orbital in a Woods–Saxon potential. It works near closed shells and fails when configuration mixing or deformation dominates (Lecture 15). Spectroscopic factors from transfer or knockout measure fragmentation of that single-particle strength; quenching relative to independent-particle estimates is common and partly a reaction-theory issue (Lecture 21).

Near drip lines, separation energies of a few hundred kilo-electronvolts make continuum coupling mandatory: resonances replace bound orbitals. Halo candidates revisit Lecture 7's exterior-probability theme. Always cross-check lecture $I^\pi$ assignments against evaluated data for a few odd-$A$ neighbours to see where the simple rule still holds.

### Depth, radius, and diffuseness trade-offs

Woods–Saxon parameters are correlated: a deeper, narrower well can mimic a shallower, wider one for a single eigenvalue. Fitting several isotopic chains and both neutron and proton orbitals reduces that ambiguity. Spin–orbit depth is additionally constrained by splitting systematics from Lecture 12.

### Resonance widths

Unbound orbitals acquire widths $\Gamma$. A level listed with $E > 0$ in a naive bound-state solver is not a physical state until a continuum method assigns a resonance energy and width. Halo candidates combine small $S_n$ with large radii: revisit Lecture 7's exterior probability for intuition.

### Parameter sensitivity

Vary the Woods–Saxon depth by 5% at fixed radius and watch a weakly bound orbital's separation energy move by hundreds of kilo-electronvolts. Near the drip line that shift can unbind the state entirely. Conversely, a deeply bound orbital barely moves. This sensitivity explains why continuum methods are mandatory for halo candidates yet optional for deeply bound closed-shell orbitals.

Assign $I^\pi$ for $^{17}$O, $^{41}$Ca, and $^{209}$Pb using a filling diagram, then check evaluated data. Where the assignment works, the extreme single-particle picture is validated; where multiple nearby states share strength, Lecture 15 collectivity or configuration mixing is already leaking into the ground state. Keep both outcomes as expected, not as embarrassments.

The Woods–Saxon model is the usable mean field for $I^\pi$ assignments. Its parameters encode saturation scales from Lecture 2 and its failures encode correlation physics from Lectures 14–15.

In practice, rework one numerical estimate from the lecture with a different parameter set and compare the shift to the quoted experimental uncertainty. If the shift exceeds the uncertainty, the estimate is teaching a scale, not delivering a fit. That distinction keeps theoretical cartoons honest when they sit beside evaluated data tables and modern many-body calculations. Along the course arc, write one sentence linking this chapter backward and one forward: the discipline of those two sentences is as important as any single formula. Examination problems rarely ask for a literature review, but they do ask for the scale argument that literature reviews presuppose.

## Synthesis problem

Write a half-page note that (i) restates the chapter's central scale or selection rule in one equation, (ii) evaluates it numerically for one concrete nucleus or energy, and (iii) names the neighbouring lecture that uses the result. Keep the note free of research-frontier speculation; the goal is fluency with the lecture physics itself. If an assumption fails (Born approximation, spherical mean field, allowed transition, one-dimensional barrier), state the failure mode in a final sentence. That habit converts passive reading into examination-ready understanding and makes the later research-frontier box read as an extension rather than a replacement.

**Research frontier: continuum shell structure and student projects**

The Woods–Saxon extreme single-particle model of Lecture 13 remains the first interpretation of odd-$A$ ground-state $I^\pi$, but near drip lines the continuum and particle decay widths must be included. Halo nuclei and unbound resonances require open quantum-system methods; spectroscopic factors extracted from knockout and transfer are often quenched relative to independent-particle estimates [43, 51]. Ab initio and density-functional approaches aim to predict drip lines and $S_n$ surfaces before experiment reaches them [44]. Uncertainties that still matter include the continuum discretisation in theoretical models, the reaction-theory corrections needed to extract spectroscopic factors, and incomplete mass and lifetime data along the most exotic isotopic chains. The lecture's single-particle language is therefore a starting map, not a finished atlas, for nuclei with small separation energies.

Near the drip line, even the definition of a single-particle energy becomes subtle because resonances have widths. Open-system formulations replace bound orbitals with Gamow or Berggren bases. Keeping that distinction clear prevents over-interpreting a Woods–Saxon level diagram for nuclei with $S_n$ of only a few hundred keV.

Distinguishing narrow resonances from true bound orbitals is essential before assigning lecture-style $I^\pi$ labels near the drip line.

*Student directions.* (1) Potential exercise: for a Woods–Saxon profile, plot $V(r)$ and estimate the 10%–90% surface thickness $t = 4a \ln 3$. (2) Data check: assign $I^\pi$ for $^{17}$O and $^{15}$N and verify against ENSDF [20]. (3) Discussion: explain why $^{61}$Ni needs configuration mixing even though a simple last-neutron rule exists.

## 1.13 Problems with solutions

**Problem 13.1 — Woods–Saxon radius**

For $^{208}$Pb with $r_0 = 1.25\,\text{fm}$, compute $R = r_0 A^{1/3}$. If $a = 0.65\,\text{fm}$, estimate the 10%–90% surface thickness $t = 4a \ln 3$.

**Solution 13.1**

$$A^{1/3} = 208^{1/3} \approx 5.924, \qquad R = 1.25 \times 5.924 \approx 7.40\,\text{fm}.$$

The surface thickness is

$$t = 4a \ln 3 = 4 \times 0.65 \times \ln 3 \approx 2.86\,\text{fm},$$

which is the Woods–Saxon 10%–90% surface thickness. It is not a neutron-skin thickness (the neutron–proton radius difference) [1, 6, 10].

**Problem 13.2 — Ground-state $J^\pi$**

Predict $I^\pi$ for $^{17}$O and for $^{40}$Ca in the extreme single-particle model.

**Solution 13.2**

$^{17}$O: unpaired neutron in $1d_{5/2}$ ($\ell = 2$, $j = \frac{5}{2}$) $\Rightarrow \frac{5}{2}^+$. $^{40}$Ca: doubly magic even–even $\Rightarrow 0^+$ [6, 20].

**Problem 13.3 — $^{15}$N configuration**

Write the proton and neutron occupations of $^{15}$N and deduce $I^\pi$.

**Solution 13.3**

Neutrons: closed through $1p_{1/2}$ ($N = 8$). Protons: $(1s_{1/2})^2(1p_{3/2})^4(1p_{1/2})^1$. Unpaired proton in $1p_{1/2} \Rightarrow I^\pi = \frac{1}{2}^-$ [6, 20].

**Problem 13.4 — Odd–odd multiplet**

An unpaired $d_{5/2}$ proton and an unpaired $p_{1/2}$ neutron form an odd–odd configuration. List the allowed $I^\pi$ values and state what additional physics is needed to choose the ground member.

**Solution 13.4**

$$|j_p - j_n| = 2, \qquad j_p + j_n = 3,$$

so $I = 2, 3$. Parity $\pi = (-1)^{2+1} = -$, hence $2^-$ and $3^-$. Residual proton–neutron interactions (guided empirically by Nordheim rules) select which of these is the ground state [19, 6].

# Bibliography


[1] R. A. Dunlap, *An Introduction to the Physics of Nuclei and Particles* (2nd ed.), IOP Publishing, Bristol (2023), DOI: 10.1088/978-0-7503-6094-4, Ch. 3 (Nuclear composition and size).

[2] W. Demtröder, *Nuclear and Particle Physics*, Undergraduate Lecture Notes in Physics, Springer, Cham (2023).

[3] S. Petrera, *Problems and Solutions in Nuclear and Particle Physics*, UNITEXT for Physics, Springer, Cham (2019).

[4] F. Terranova, *A Modern Primer in Particle and Nuclear Physics*, Oxford University Press (2021).

[5] S. D'Auria, *Introduction to Nuclear and Particle Physics*, Undergraduate Lecture Notes in Physics, Springer, Cham (2018).

[6] K. S. Krane, *Introductory Nuclear Physics*, Wiley, New York (1988).

[7] R. Hofstadter, "Electron scattering and nuclear structure," Rev. Mod. Phys. **28**, 214 (1956).

[8] H. F. Ehrenberg, R. Hofstadter, U. Meyer-Berkhout, D. G. Ravenhall, and S. E. Sobottka, "High-Energy Electron Scattering and the Charge Distribution of Carbon-12 and Oxygen-16," Phys. Rev. **113**, 666 (1959).

[9] H. Yukawa, "On the interaction of elementary particles. I," Proc. Phys.-Math. Soc. Japan **17**, 48 (1935).

[10] R. D. Woods and D. S. Saxon, "Diffuse surface optical model for nucleon-nuclei scattering," Phys. Rev. **95**, 577 (1954).

[11] H. G. J. Moseley, "The high-frequency spectra of the elements," Phil. Mag. **26**, 1024 (1913); **27**, 703 (1914).

[12] C. F. von Weizsäcker, "Zur Theorie der Kernmassen," Z. Phys. **96**, 431 (1935).

[13] P. Cappellaro, *Introduction to Applied Nuclear Physics* (MIT OpenCourseWare / LibreTexts), CC BY-NC-SA 4.0.

[14] J.-L. Basdevant, J. Rich, and M. Spiro, *Fundamentals in Nuclear Physics: From Nuclear Structure to Cosmology*, Springer, New York (2005).

[15] D. Tong, *Particle Physics*, Lecture notes (University of Cambridge / CERN school notes).

[16] M. G. Mayer, "On closed shells in nuclei. II," Phys. Rev. **75**, 1969 (1949).

[17] O. Haxel, J. H. D. Jensen, and H. E. Suess, "On the "magic numbers" in nuclear structure," Phys. Rev. **75**, 1766 (1949).

[18] T. Schmidt, "Über die magnetischen Momente der Atomkerne," Z. Phys. **106**, 358 (1937).

[19] L. W. Nordheim, "On spins, moments, and shells in nuclei," Phys. Rev. **78**, 294 (1950).

[20] Evaluated Nuclear Structure Data File (ENSDF), National Nuclear Data Center, Brookhaven National Laboratory, `https://www.nndc.bnl.gov/ensdf/`.

[21] NuDat 3, National Nuclear Data Center, Brookhaven National Laboratory, `https://www.nndc.bnl.gov/nudat3/`.

[22] N. J. Stone, "Table of nuclear magnetic dipole and electric quadrupole moments," At. Data Nucl. Data Tables **90**, 75 (2005); updated compilations at NNDC.

[23] W. N. Cottingham and D. A. Greenwood, *An Introduction to Nuclear Physics* (2nd ed.), Cambridge University Press, Cambridge (2001).

[24] H. Geiger and J. M. Nuttall, "The ranges of the $\alpha$ particles from the radioactive substances," Phil. Mag. **22**, 613 (1911).

[25] G. Gamow, "Zur Quantentheorie des Atomkernes," Z. Phys. **51**, 204 (1928).

[26] R. W. Gurney and E. U. Condon, "Wave mechanics and radioactive disintegration," Nature **122**, 439 (1928); Phys. Rev. **33**, 127 (1929).

[27] M. Wang, W. J. Huang, F. G. Kondev, G. Audi, and S. Naimi, "The AME 2020 atomic mass evaluation (II). Tables, graphs and references," Chin. Phys. C **45**, 030003 (2021).

[28] Laboratoire National Henri Becquerel (LNHB), Recommended decay data, `http://www.lnhb.fr/nuclear-data/nuclear-data-table/`.

[29] L. M. Langer, R. D. Moffat, and H. C. Price, Jr., "Low energy beta-ray spectra: $P^{32}$ and $Cu^{64}$," Phys. Rev. **76**, 1725 (1949).

[30] L. M. Langer and H. C. Price, Jr., "Shapes of the beta-spectra of the forbidden transitions of $Sb^{124}$, $Rb^{86}$, $Sr^{89}$, $Y^{91}$, and $Cs^{137}$," Phys. Rev. **75**, 1769 (1949).

[31] D. C. Camp and L. M. Langer, "The shape of the $^{66}$Ga positron spectrum and the contribution from $0^+ \to 0^+$ transitions," Phys. Rev. **129**, 1782 (1963).

[32] H. C. Verma, *Nuclear Physics: Fundamentals and Applications*, NPTEL/IIT Kanpur lecture series, `https://hcverma.in/ncl_phy_lectures`.

[33] International Atomic Energy Agency, *LiveChart of Nuclides*, evaluated structure, decay, reaction, and fission-yield data, `https://www-nds.iaea.org/relnsd/vcharthtml/VChartHTML.html`.

[34] T. Kibédi, T. W. Burrows, M. B. Trzhaskovskaya, P. M. Davidson, and C. W. Nestor, Jr., "Evaluation of theoretical conversion coefficients using BrIcc," Nucl. Instrum. Methods Phys. Res. A **589**, 202 (2008), DOI: 10.1016/j.nima.2008.02.051.

[35] D. A. Brown *et al.*, "ENDF/B-VIII.0: The 8th major release of the nuclear reaction data library with CIELO-project cross sections, new standards and thermal scattering data," Nucl. Data Sheets **148**, 1 (2018), DOI: 10.1016/j.nds.2018.02.001.

[36] B. Acharya *et al.*, "Solar fusion III: New data and theory for hydrogen-burning stars," Rev. Mod. Phys. **97**, 035002 (2025), DOI: 10.1103/8lm7-gs18.

[37] S. N. Ghoshal, "An experimental verification of the theory of compound nucleus," Phys. Rev. **80**, 939 (1950), DOI: 10.1103/PhysRev.80.939.

[38] D. Adhikari *et al.* (PREX Collaboration), "Accurate determination of the neutron skin thickness of $^{208}$Pb through parity-violation in electron scattering," Phys. Rev. Lett. **126**, 172502 (2021), DOI: 10.1103/PhysRevLett.126.172502.

[39] B. T. Reed, F. J. Fattoyev, C. J. Horowitz, and J. Piekarewicz, "Implications of PREX-II on the equation of state of neutron-rich matter," Phys. Rev. Lett. **126**, 172503 (2021), DOI: 10.1103/PhysRevLett.126.172503.

[40] B. Hu *et al.*, "Ab initio predictions link the neutron skin of $^{208}$Pb to nuclear forces," Nature Phys. **18**, 1196 (2022), DOI: 10.1038/s41567-022-01715-8.

[41] E. Epelbaum, H.-W. Hammer, and U.-G. Meißner, "Modern theory of nuclear forces," Rev. Mod. Phys. **81**, 1773 (2009), DOI: 10.1103/RevModPhys.81.1773.

[42] H.-W. Hammer, S. König, and U. van Kolck, "Nuclear effective field theory: Status and perspectives," Rev. Mod. Phys. **92**, 025004 (2020), DOI: 10.1103/RevModPhys.92.025004.

[43] T. Otsuka, A. Gade, O. Sorlin, T. Suzuki, and Y. Utsuno, "Evolution of shell structure in exotic nuclei," Rev. Mod. Phys. **92**, 015002 (2020), DOI: 10.1103/RevModPhys.92.015002.

[44] H. Hergert, S. K. Bogner, T. D. Morris, A. Schwenk, and K. Tsukiyama, "The in-medium similarity renormalization group: A novel ab initio method for nuclei," Phys. Rep. **621**, 165 (2016), DOI: 10.1016/j.physrep.2015.12.007.

[45] J. M. Lattimer and M. Prakash, "The equation of state of hot, dense matter and neutron stars," Phys. Rep. **621**, 127 (2016), DOI: 10.1016/j.physrep.2015.12.005.

[46] J. M. Lattimer, "Neutron stars and the nuclear matter equation of state," Annu. Rev. Nucl. Part. Sci. **71**, 433 (2021), DOI: 10.1146/annurev-nucl-102419-124827.

[47] B. P. Abbott *et al.* (LIGO Scientific Collaboration and Virgo Collaboration), "GW170817: Observation of gravitational waves from a binary neutron star inspiral," Phys. Rev. Lett. **119**, 161101 (2017), DOI: 10.1103/PhysRevLett.119.161101.

[48] M. J. Dolinski, A. W. P. Poon, and W. Rodejohann, "Neutrinoless double-beta decay: Status and prospects," Annu. Rev. Nucl. Part. Sci. **69**, 219 (2019), DOI: 10.1146/annurev-nucl-101918-023407.

[49] M. Agostini, G. Benato, J. A. Detwiler, J. Menéndez, and F. Vissani, "Toward the discovery of matter creation with neutrinoless $\beta\beta$ decay," Rev. Mod. Phys. **95**, 025002 (2023), DOI: 10.1103/RevModPhys.95.025002.

[50] P. Gysbers *et al.*, "Discrepancy between experimental and theoretical $\beta$-decay rates resolved from first principles," Nature Phys. **15**, 428 (2019), DOI: 10.1038/s41567-019-0450-7.

[51] H. L. Crawford, K. Fossez, S. König, and A. Spyrou, "A vision for the science of rare isotopes," Annu. Rev. Nucl. Part. Sci. **74**, 141 (2024), DOI: 10.1146/annurev-nucl-121423-091501.

[52] Nuclear Science Advisory Committee, *A New Era of Discovery: The 2023 Long Range Plan for Nuclear Science*, U.S. Department of Energy and National Science Foundation (2023), `https://nuclearsciencefuture.org/`.

[53] S. A. Giuliani, Z. Matheson, W. Nazarewicz, E. Olsen, P.-G. Reinhard, J. Sadhukhan, B. Schuetrumpf, N. Schunck, and P. Schwerdtfeger, "Colloquium: Superheavy elements: Oganesson and beyond," Rev. Mod. Phys. **91**, 011001 (2019), DOI: 10.1103/RevModPhys.91.011001.

[54] N. Schunck and D. Regnier, "Theory of nuclear fission," Prog. Part. Nucl. Phys. **125**, 103963 (2022), DOI: 10.1016/j.ppnp.2022.103963.

[55] I. Counts, J. Hur, D. P. L. Aude Craik, H. Jeon, C. Leung, J. C. Berengut, A. Geddes, A. Kawasaki, W. Jhe, and V. Vuletić, "Evidence for nonlinear isotope shift in $Yb^+$ search for new boson," Phys. Rev. Lett. **125**, 123002 (2020), DOI: 10.1103/PhysRevLett.125.123002.

[56] I. Angeli and K. P. Marinova, "Table of experimental nuclear ground state charge radii: An update," At. Data Nucl. Data Tables **99**, 69 (2013), DOI: 10.1016/j.adt.2011.12.006.

[57] S. Kraemer *et al.*, "Observation of the radiative decay of the $^{229}$Th nuclear clock isomer," Nature **617**, 706 (2023), DOI: 10.1038/s41586-023-05894-z.